Microrheology of red blood cell membranes using dynamic scattering microscopy

M. Shahrooz Amin[1], YoungKeun Park[1], Niyom Lue[1], Ramachandra R. Dasari[1], Kamran Badizadegan[1,2], Michael S. Feld[1], and Gabriel Popescu[1,3]

[1]*G. R. Harrison Spectroscopy Laboratory, Massachusetts Institute of Technology, Cambridge, Massachusetts 02139*
[2]*Departments of Pathology and Health Sciences and Technology, Harvard Medical School and Massachusetts General Hospital, Boston, MA 02114*
[3] *Current address: Quantitative Light Imaging Laboratory, Department of Electrical and Computer Engineering, Beckman Institute for Advanced Science & Technology, University of Illinois at Urbana-Champaign, Urbana, IL 61801*
gpopescu@uiuc.edu

Abstract: We employ a novel optical technique, dynamic scattering microscopy (DSM), to extract the frequency dependence of the viscoelastic modulus associated with the red blood cell membrane. This approach applies the principle of dynamic light scattering to micro beads attached to the red blood cell membrane in thermal fluctuation. This allows for high-throughput characterization of a large number of cells simultaneously, which represents a significant advantage over current methods. The results in terms of the effective loss and storage moduli indicate the generic behavior of a viscoelastic material, characterized by power laws with exponents between 0 and 1.

©2007 Optical Society of America

OCIS codes: (180.018) Microscopy, (170) Medical optics and biotechnology: (1470) Blood or tissue constituent monitoring dynamic scattering micoscopy

References and links

1. F. Brochard and J. F. Lennon, "Frequency spectrum of the flicker phenomenon in erythrocytes," J. Phys. **36**, 1035-1047 (1975).
2. H. Engelhardt, H. Gaub, and E. Sackmann, "Viscoelastic properties of erythrocyte membranes in high-frequency electric fields," Nature **307**, 378-380 (1984).
3. N. Gov, "Membrane undulations driven by force fluctuations of active proteins," Phys. Rev. Lett. **93**, 268104 (2004).
4. N. Gov, A. Zilman, and S. Safran, "Cytoskeleton confinement of red blood cell membrane fluctuations," Biophys. J. **84**, 486A-486A (2003).
5. S. Levin and R. Korenstein, "Membrane fluctuations in erythrocytes are linked to Mgatp-dependent dyanamic assembly of the membrane skeleton," Biophys. J. **60**, 733-737 (1991).
6. J. Liu, G. Lykotrafitis, M. Dao, and S. Suresh, "Cytoskeletal dynamics of human erythrocyte," Proc Natl Acad Sci U S A **104**, 4937-4942 (2007).
7. R. Mukhopadhyay, G. Lim, and M. Wortis, "Echinocyte shapes: bending, stretching, and shear determine spicule shape and spacing," Biophys. J. **82**, 1756-1772 (2002).
8. G. Popescu, K. Badizadegan, R. R. Dasari, and M. S. Feld, "Observation of dynamic subdomains in red blood cells," J. Biomed. Opt. Lett. **11**, 040503 (2006).
9. G. Popescu, T. Ikeda, C. A. Best, K. Badizadegan, R. R. Dasari, and M. S. Feld, "Erythrocyte structure and dynamics quantified by Hilbert phase microscopy," J. Biomed. Opt. Lett. **10**, 060503 (2005).
10. G. Popescu, T. Ikeda, K. Goda, C. A. Best-Popescu, M. Laposata, S. Manley, R. R. Dasari, K. Badizadegan, and M. S. Feld, "Optical measurement of cell membrane tension," Phys. Rev. Lett. **97**, 218101 (2006).
11. C. F. Schmidt, K. Svoboda, N. Lei, I. B. Petsche, L. E. Berman, C. R. Safinya, and G. S. Grest, "Existence of a flat phase in red cell membrane skeletons," Science **259**, 952-955 (1993).
12. M. P. Sheetz, and S. J. Singer, "On the mechanism of ATP-induced shape changes in human erythrocyte membranes. I. The role of the spectrin complex," J Cell Biol **73**, 638-646 (1977).
13. S. Tuvia, A. Almagor, A. Bitler, S. Levin, R. Korenstein, and S. Yedgar, "Cell membrane fluctuations are regulated by medium macroviscosity: evidence for a metabolic driving force," Proc. Natl. Acad. Sci. U. S. A. **94**, 5045-5049 (1997).

14. A. Zilker, M. Ziegler, and E. Sackmann, "Spectral-analysis of erythrocyte flickering in the 0.3-4-Mu-M-1 regime by microinterferometry combined with fast image-processing," Phys. Rev. A **46**, 7998-8002 (1992).
15. G. Popescu, Y. K. Park, R. R. Dasari, K. Badizadegan, and M. S. Feld, "Coherence properties of red blood cell membrane motions," Phys. Rev. E. **76**, 031902 (2007).
16. R. Lipowski and E. Sackman, *Handbook of Biological Physics* (Elsevier, 1995).
17. C. A. Best, "Fatty acid ethyl esters and erythrocytes: metabolism and membrane effects, Ph.D. Thesis," in *Pharmacy and Health Sciences* (Northeastern University, Boston, 2005).
18. S. Suresh, "Mechanical response of human red blood cells in health and disease: Some structure-property-function relationships," J. Mater. Res. **21**, 1871-1877 (2006).
19. G. Bao and S. Suresh, "Cell and molecular mechanics of biological materials," Nat. Mater **2**, 715-725 (2003).
20. D. E. Discher, N. Mohandas, and E. A. Evans, "Molecular maps of red cell deformation: hidden elasticity and in situ connectivity," Science **266**, 1032-1035 (1994).
21. M. Dao, C. T. Lim, and S. Suresh, "Mechanics of the human red blood cell deformed by optical tweezers," J. Mech. Phys. Solids **51**, 2259-2280 (2003).
22. M. Puig-de-Morales, K. T. Turner, J. P. Butler, J. J. Fredberg, and S. Suresh, "Viscoelasticity of the human red blood cell," J. Appl. Physiol. **293**, 597-605 (2007).
23. N. Gov, A. G. Zilman, and S. Safran, "Cytoskeleton confinement and tension of red blood cell membranes," Phys. Rev. Lett. **90**, 228101 (2003).
24. L. C. L. Lin and F. L. H. Brown, "Brownian dynamics in Fourier space: Membrane simulations over long length and time scales," Phys. Rev. Lett. **93,** 256001 (2004).
25. L. C. L. Lin, N. Gov, and F. L. H. Brown, "Nonequilibrium membrane fluctuations driven by active proteins," J. Chem. Phys. **124**, 074903 (2006).
26. M. T. Valentine, A. K. Popp, P. D. Kaplan, and D. A. Weitz, "Microscope-based static light scattering apparatus," Opt. Lett. **26**, 890892 (2001).
27. W. J. Cottrell, J. D. Wilson, and T. H. Foster, "Microscope enabling multimodality imaging, angle-resolved scattering, and scattering spectroscopy," Opt. Lett. **32**, 2348-2350 (2007).
28. J. C. Crocker, M. T. Valentine, E. R. Weeks, T. Gisler, P. D. Kaplan, A. G. Yodh, and D. A. Weitz, "Two-point microrheology of inhomogeneous soft materials," Phys. Rev. Lett. **85**, 888-891 (2000).
29. A. J. Levine and T. C. Lubensky, "One- and two-particle microrheology," Phys. Rev. Lett. **85**, 1774-1777 (2000).
30. T. G. Mason, and D. A. Weitz, "Optical measurements of frequency-dependent linear viscoelastic moduli of complex fluids," Phys. Rev. Lett. **74**, 1250-1253 (1995).
31. B. J. Bern and R. Pecora, *Dynamic light scattering with applications to chemistry, biology and Phys.* (Wiley, New York, 1976).
32. G. Popescu and A. Dogariu, "Dynamic light scattering in localized coherence volumes," Opt. Lett. **26**, 551-553 (2001).
33. N. A. Lange, *Lange's Handbook of Chemistry* (McGraw-Hill, 1999).
34. S. J. Johnson, T. M. Bayerl, W. H. Wo, H. Noack, J. Penfold, R. K. Thomas, D. Kanellas, A. R. Rennie, and E. Sackmann, "Coupling of spectrin and polylysine to phospholipid monolayers studied by specular reflection of Neutrons," Biophys. J. **60**, 1017-1025 (1991).
35. L. H. Deng, X. Trepat, J. P. Butler, E. Millet, K. G. Morgan, D. A. Weitz, and J. J. Fredberg, "Fast and slow dynamics of the cytoskeleton," Nat. Mater. **5**, 636-640 (2006).
36. E. Helfer, S. Harlepp, L. Bourdieu, J. Robert, F. C. MacKintosh, and D. Chatenay, "Microrheology of Biopolymer-Membrane Complexes," Phys. Rev. Lett. **85**, 457-460 (2000).
37. L. H. Deng, N. J. Fairbank, B. Fabry, P. G. Smith, and G. N. Maksym, "Localized mechanical stress induces time-dependent actin cytoskeletal remodeling and stiffening in cultured airway smooth muscle cells," Am. J. Physiol.:Cell Physiol. **287**, C440-C448 (2004).
38. B. Fabry, G. N. Maksym, J. P. Butler, M. Glogauer, D. Navajas, and J. J. Fredberg, "Scaling the microrheology of living cells," Phys. Rev. Lett. **8714**, art. no.-148102 (2001).

1. Introduction

The structure and dynamics of red blood cells (RBCs) have been studied extensively for two main reasons [1-15]. First, since this type of cell can be approximated by a 2D bilayer-cytoskeleton viscoelastic membrane that encloses a homogeneous hemoglobin solution, it is a suitable model for cell membrane biophysics [16]. Second, understanding the interaction between the lipid bilayer and the cytoskeletal protein (spectrin) network provides insight into the overall mechanical properties of the cells, which impacts their function in health and disease. Physiologically, RBCs must withstand large deformations during multiple passages through the microvasculature and spleen sinusoids. The RBC deformability is progressively diminished with age, which eventually determines the cell removal from the circulation [17].

Diseases such as spherocytosis, malaria, and sickle cell anemia affect both the RBC morphology and their dynamic properties [18].

In recent years, a number of different techniques have been used to assess the rheology of live cells [19]. Among them, pipette aspiration [20], electric field deformation [2], and optical tweezers [21] provided quantitative information about the shear and bending moduli of RBC membranes in static conditions. However, dynamic, frequency-dependent knowledge of the RBC mechanical response is currently very limited [22]. Red blood cell membrane fluctuations have been investigated intensively, as they offer a potential window into the structure, dynamics, and function of the cell1, [3, 5, 10, 13, 23-25]. In spite of these efforts, the interaction between the lipid bilayer and underlying cytoskeleton network and how it impacts on the overall mechanical properties of the cell is insufficiently known.

Here, we employ a new optical technique, referred to as dynamic scattering microscopy (DSM), to quantify the microrheological properties of live cell membranes. Static light scattering have been accessed in a microscope-based system previously [26, 27]. To our knowledge, this is the first time that dynamics light scattering is performed using microscopy platform. Using DSM, we measure the time-fluctuating irradiance scattered at a certain angle by micro beads conjugated to RBC membranes. By employing the fluctuation-dissipation theorem and generalized Stokes-Einstein relationship, this dynamic scattering signal is translated into an effective frequency-dependent 3D complex shear modulus $G(\omega)$, as in previous microrheology studies applied to 3D complex fluids [28-30].

2. Experimental results

2.1 Experimental set-up

The experimental setup combines dynamic light scattering [31] with typical inverted microscopy and is described in Fig. 1. Monochromatic light emitted by an Ar^{++} laser (λ=514 nm) is used to illuminate the sample. To ensure full spatial coherence, the light from the source is coupled into a single mode fiber and further collimated by a fiber collimator (FC). The Olympus IX 71 inverted microscope produces a magnified image of the sample at the plane IP. The lens L1 (f = 200 mm), creates the Fourier transform of the sample field at plane FP. This plane is imaged at the CMOS camera plane via the beam splitter BS. The lens L_2 (f = 250mm) and mirror M act as a folded 4-f system, which projects the optical field at the plane FP onto the CMOS plane, with unit magnification. The 40x objective lens (NA=0.75) provides a field of view of 400μm, which allows for a high number (in the order of 1,000) of red blood cells to be imaged simultaneously. The 8 bit CMOS camera (C8021, Hamamatsu Co.) records angular scattering from the sample over a wide angle interval of (-32°, 32°). In order to prevent CMOS camera saturation due to strong low-angle scattering, we placed a spatial filter at the plane FP to obstruct the DC term. A computer was used to acquire the raw data from the camera. By employing a full-field detector at the Fourier plane of the sample field, a broad spectrum of spatial frequencies associated with the scattered field can be examined. Throughout our experiments, the CMOS acquisition rate was 256 frames per second, at a frame resolution of 256 $\times$ 256 pixels.
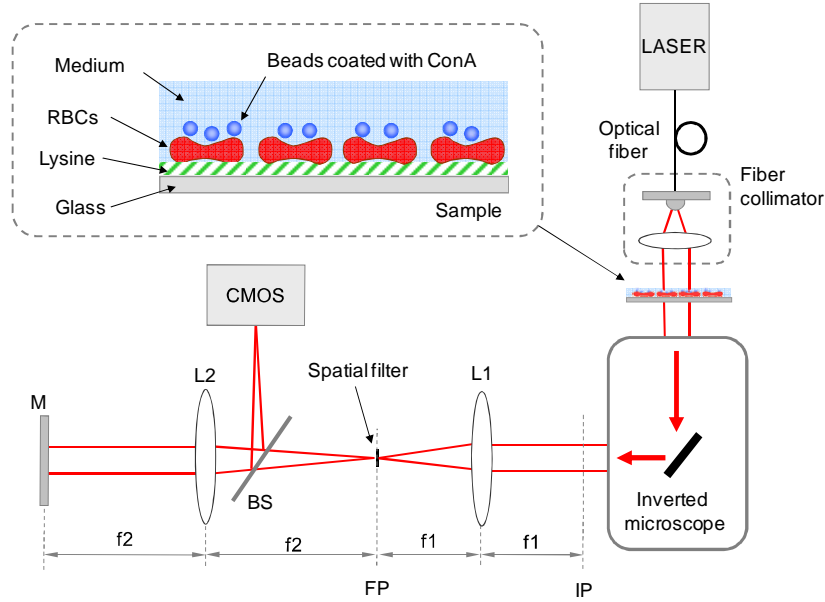
Fig. 1. DSM experimental setup. M: Mirror, L1,2: lenses, f1,2: focal length of lense 1,2, BS: beam splitter, IP: image plane, FP: Fourier plane

2.2 Experimental analysis

In order to demonstrate the ability of DSM to extract dynamic information from fluids, we measured the angular distribution of light scattering from polystyrene micro beads undergoing Brownian motion in Newtonian fluids, i.e. in glycerol solutions of various concentrations. Figure 2(a) shows a single frame of the angular scattering map associated with 0.26 μm diameter beads (10% solids, Duke Scientific Co.,) undergoing Brownian motion in water. The spatial filtering of the DC component is clearly visible. Figure 2(b) shows an example of the dynamic scattering signal of a single point on the ring, which is characterized by the polar angle θ and the azimuthal angle φ. For a given scattering angle θ, the modulus of the scattering vector is $q = (4\pi/\lambda)\sin(\theta/2)$, and the power spectrum is obtained by averaging the power spectra associated with all the pixels within the ring of equal φ values. For studying simple fluids, the power spectra were fitted with a Lorentzian function, which provided the width Δω and amplitude A of the distribution [32],

$$P(\omega) = \frac{A}{\Delta\omega} \frac{1}{1+(\omega/\Delta\omega)^2} .$$

(1)

In Eq. (1), $\Delta\omega = Dq^2$, where the diffusion coefficient $D = k_B T / 6\pi\eta a$, with k_B the Boltzmann constant, T the absolute temperature, η the viscosity and the radius of the bead.
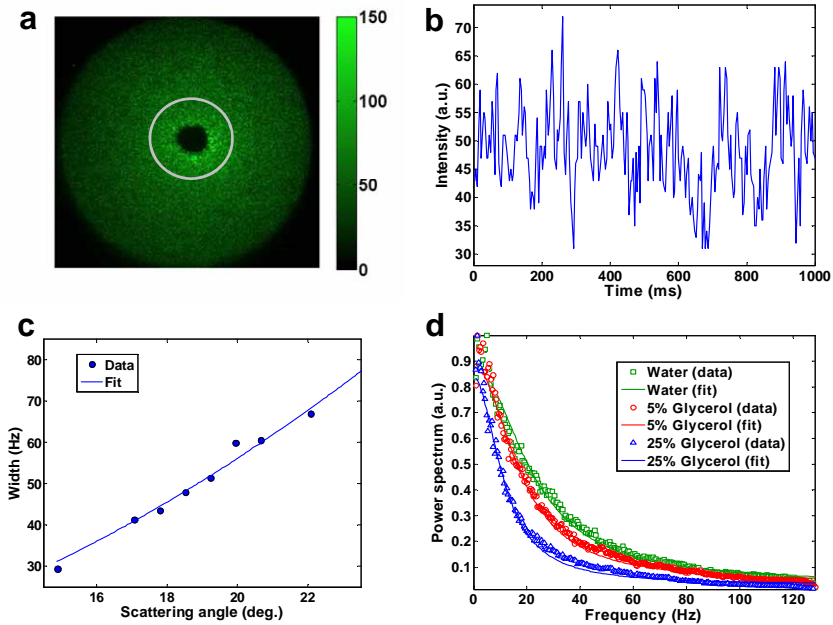
Fig. 2. (a). Single frame angular scattering map in DSM. (b). Intensity fluctuations associated with the angle shown in a) over 1 sec (256 frames). (c). The widths of the power spectra vs. scattering angle and fit with the theoretical model. (d). Power spectra for liquids of various viscosities, as indicated. The solid lines show the theoretical fit.

2.3 *Results from beads*

Figure 2(c) shows the widths of the power spectra obtained at various scattering angles, which indicates a very good agreement with the theoretical values. We found that, for scattering at various angles, particles of various diameters, and fluids of different viscosities, the width of the measured power spectrum was a factor of 2/3 of what was expected. This consistent calibration factor needed in our DSM measurements can be explained by assuming that, due to the high numerical aperture of the microscope, the motion of the scattering particles that contribute most significantly to the dynamic signal takes place in the (x, y) plane, i.e. perpendicular to the optical axis. Thus, the factor of 2/3 reflects the ratio between the mean squared displacements of a particle jittering in 2D vs. 3D space. Thus, throughout our measurements, we incorporated this constant calibration factor.

Figure 2(d) depicts the measured effect of the solvent viscosity on the characteristic width of the power spectrum for beads of radius *a=0.13 μm*. From the Lorentzian fit, we extracted the values for the viscosity of the fluid at temperature T=298 K: η =0.987±0.013 mPa·s (water), η =1.2 mPa·s±0.1 (5% glycerol), and η =1.9±0.1 mPa·s (25% glycerol), which agree very well with the expected values [33]. These results demonstrate the ability of DSM to quantify the mechanical properties of fluids.

2.4 *Experimental procedure of determining the viscoelastic behavior of red blood cells*

Using DSM, we quantified the viscoelastic properties of RBCs by recording the dynamic scattering signal from 0.13 μm radius beads conjugated to the membranes. In order to prevent the cells from undergoing translational motions, we treated the glass substrate with polylysine hydrobromide P1274 (Sigma Aldrich Co.). The polylysine solution was poured onto the glass dish containing cells and allowed to incubate for approximately two hours at room temperature. Prior to the DSM experiment, the unattached RBCs were washed with PBS three times. Polylysine creates positive charge on the cover glass, which then attracts and affixes the

negatively charged cell membrane [34]. The effectiveness of polylysine is demonstrated in Fig. 3, where it is shown that the width of the power spectrum is significantly narrower when the RBCs are fixed to the substrate. This narrowing of the power spectrum is due to suppressing the translation motion of the RBCs.

The beads were coated with the protein Concanavalin A (Con A, Sigma Aldrich Co.). The 1 mg/ml phosphate buffered saline (PBS) solution of ConA was mixed with the beads and allowed to incubate at the room temperature. After the attachment of RBCs onto the glass substrate containing polylysine, solution containing the coated beads was added. Prior to the DSM experiment, any unattached beads were washed with PBS several times. Thus, by recording the dynamic light scattering originating exclusively from the fluctuating particles that are attached to the RBC membranes, an effective complex shear modulus can be obtained by following the procedure used in passive microrheology [30].

2.5 *Power spectrum from the red blood cells*

The light scattered by the thermally fluctuating membranes can also generate dynamic light scattering, which mixes with the scattering from the particles. In order to quantify this effect, we performed DSM measurements of RBCs attached to the cover glass, but without attaching particles to the cells. As can be seen in Fig. 3, the scattering from the RBC membranes alone is very weak compared to the scattering from particles and, therefore, can be ignored. This is also supported by the fact that each RBC contains on average two or more beads, which produce stronger scattering than the membrane alone [Fig. 3(b)]. Furthermore, due to the large number of scattering micro beads, the Gaussian statistics of dynamic light scattering holds [31]. In order to remove the electronic noise of the CMOS camera that affects the signal at particular frequencies, we applied filtering by fitting the power spectra with rational polynomials of the third order (using 4 fitting parameters). Thus, for the subsequent analysis, we used this fit curve instead of the data, such that the information of the original data is retained but the effect of the noise is removed. We chose this type of fitting function because it describes the data extremely well ($r^2 > 0.99$) for samples with various dynamic properties. An example of such fit is shown in Fig. 3(c).
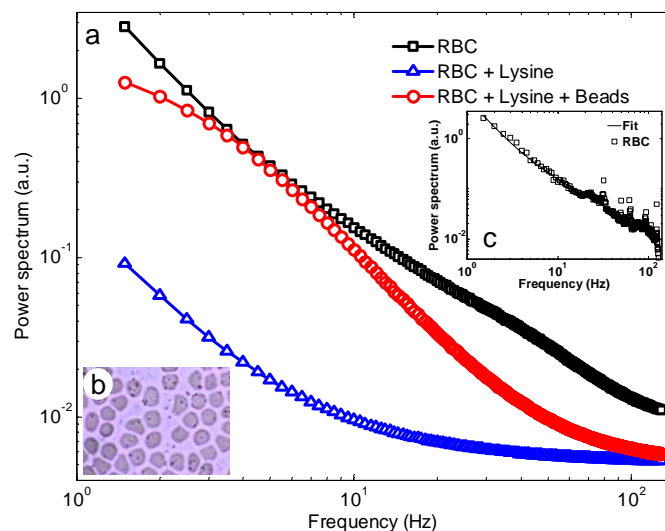

Fig. 3. (a). Power spectra associated with the dynamic scattering from RBCs in suspension, RBCs fixed on cover slips by lysine, and fixed RBCs with micro beads attached, as indicated. (b). Bright filed image of the micro beads attached to RBCs. (c). Fitting procedure to eliminate the noise peaks.

2.6 *Method of quantifying the viscoelastic behavior of the red blood cells*

From this filtered power spectrum $P(\omega)$, we extracted the effective 3D shear modulus G, as follows. First, we calculated the intensity-intensity autocorrelation $g^{(2)}(\tau)$ by Fourier transforming $P(\omega)$. The Siegert relationship connects the intensity autocorrelation function with the field autocorrelation function $g^{(1)}(\tau)$,

$$g^{(2)}(\tau)=1+\beta\left[g^{(1)}(\tau)\right]^2,\tag{2}$$

where β is the *coherence factor,* with values between 0 and 1. Due to our single light scattering conditions with high temporal and spatial coherence field, we can assume $\beta=1$. Thus, $g^{(1)}$ can be obtained from Eq. (2) and further used to infer the particle mean squared displacement $\langle\Delta r^2(\tau)\rangle$ as [31]

$$\left\langle\Delta r^2(\tau)\right\rangle=-\frac{6}{q^2}\ln\left[g^{(1)}(\tau)\right]\tag{3}$$

The power spectrum of the mean-squared displacement, $\langle\Delta r^2(\omega)\rangle$, was then obtained by taking the Fourier transform of $\langle\Delta r^2(\tau)\rangle$. The fluctuation-dissipation theorem (FDT) relates the $\langle\Delta r^2(\omega)\rangle$ to the loss response $\chi''(\omega)$,

$$\chi''(\omega)=\frac{\omega}{2k_b t}\left\langle\Delta r^2(\omega)\right\rangle\tag{4}$$

The storage response function $\chi'(\omega)$ is related to $\chi''(\omega)$ by the Kramers-Kronig relation, which expresses the causality of the system

$$\chi'(\omega)=\frac{2}{\pi}P\int_0^\infty\chi''(\xi)\frac{\xi}{\xi^2-\omega^2}d\xi\tag{5}$$

The symbol P in Eq. (5) indicates a principal value integral. The shear modulus $G(\omega)$ is related to the response function $\chi(\omega)$ by the generalized Stokes-Einstein relationship,

$$G(\omega)=\frac{1}{6\pi a}\frac{1}{\chi(\omega)}\tag{6}$$

where a=0.13 μm denotes the radius of the scattering beads.

2.7 *Viscoelastic response data from the red blood cells*

We used this procedure to measure G for different samples of RBCs attached to microscope slides. Figure 4(a) shows the average frequency dependence of the storage $G'(\omega)$ and loss $G''(\omega)$ moduli obtained from DSM measurements of 3 different RBC preparations at various scattering angles, with a total of 13 measurements. The errors indicate the sample-to-sample variation (N=13). Interestingly, over the frequency region centered on $(10,100)Hz$, the behavior of both the loss and storage moduli can be approximated well by power laws. It is well known that $G''\propto\omega^1$ describes a Newtonian fluid, while $G''\propto\omega^0$ indicates a solid behavior. Therefore, the intermediate exponent measured by our technique, $G''\propto\omega^{0.69}$, simply indicates that the membrane is a viscoelastic fluid.
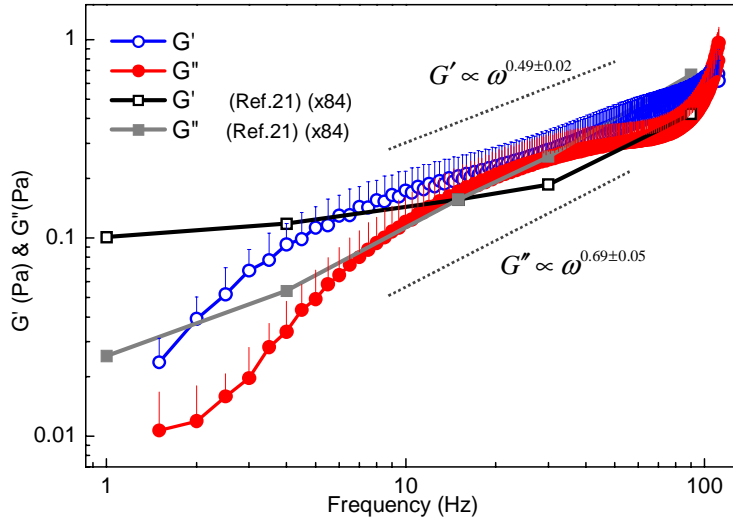
Fig. 4. DSM measurements of G vs. frequency. The dashed lines indicate power laws of different exponents, as indicated. Also shown in this figure for comparison purpose are complex shear modulus measured from magnetic twisting cytometry scaled by a factor of 84 to convert 2D in-plane shear modulus into 3D shear modulus [22]. The error bars (only upper error bars shown) are due to sample-to-sample variability (N=13).

To our knowledge, the only data published to date on the rheology of RBCs at the single-cell level is by Puig-de-Morales, *et al.* [22], which is also shown in the Fig. 4 for comparison purpose. In their experiments, magnetic beads attached to the RBC membranes are activated by external magnetic fields and the positions of beads are tracked in order to retrieve in-plane 2D complex modulus [35]. In an earlier work, 2D in-plane shear modulus was measured [22], in which RBC membrane and cytoskeleton complex is assumed as plane without thickness. Using the fluctuation-dissipation theorem and assumption that modulus $G'(\omega)$ and $G''(\omega)$ can be scaled with frequency, 2D complex shear modulus can be expressed in terms of in-plane displacement as follows [36]:

$$\left\langle \Delta r^2(\omega) \right\rangle \cong \frac{k_B T}{5\pi\omega} \frac{1}{G_{2D}(\omega)}$$

(7)

In contrast, we extract 3D shear modulus of RBC membrane, taking account in the physical thickness of the RBC membrane which consists of phospholipid bilayer and spectrin network attached to the membrane. In order to directly compare with 2D shear modulus, combining Eq. (4) and Eq. (6) yields,

$$\left\langle \Delta r^2(\omega) \right\rangle = \frac{k_B T}{3\pi\omega a} \frac{1}{G_{3D}(\omega)}$$

(8)

Thus,

$$G_{3D}(\omega)(Pa) \cong \frac{3a}{5} G_{2D}(\omega)\left(\frac{Pa}{nm}\right)$$

(9)

As we used 0.26 μm diameter probing bead, the factor between 2D shear modulus and 3D shear modulus is 84 nm, which is used for scaling the result of ref 21 in Fig. 4. The complex

modulus, $G'(\omega)$ and $G''(\omega)$ from our measurement is consistent with the previous result [22] over the intermediate frequency range in term of both absolute values and slopes. Remarkably, the power law dependence of $G''(\omega)$ reported in Ref. [22] has a value of 0.67, which agrees very well with our value of 0.69.

3. Conclusion

In summary we have presented a new optical method for extracting the viscoelastic moduli of RBC membranes. The technique relies on quantifying the thermal motion of micro beads attached to the membrane. The results compare well with those obtained by magnetic bead excitation [37, 38]. However, our approach provides the rheological information without the need for an external magnetic field. Quantitative phase imaging of RBC thermal fluctuations offers unique insight into the cell membrane properties at the cellular and sub-cellular level. By contrast to the flickering experiments, the current DSM probes a large number of cells simultaneously, which allows for an intrinsic ensemble averaging.